Structural and Kinetic Characterization of *Escherichia coli* TadA, the Wobble-Specific tRNA Deaminase[†]

Jungwook Kim,[||] Vladimir Malashkevich,[||] Setu Roday, Michael Lisbin, Vern L. Schramm, and Steven C. Almo*

Department of Biochemistry, Center for Synchrotron Biosciences, Albert Einstein College of Medicine, 1300 Morris Park Avenue, Bronx, New York 10461

ABSTRACT: The essential tRNA-specific adenosine deaminase catalyzes the deamination of adenosine to inosine at the wobble position of tRNAs. This modification allows for a single tRNA species to recognize multiple synonymous codons containing A, C, or U in the last (3′-most) position and ensures that all sense codons are appropriately decoded. We report the first combined structural and kinetic characterization of a wobble-specific deaminase. The structure of the *Escherichia coli* enzyme clearly defines the dimer interface and the coordination of the catalytically essential zinc ion. The structure also identifies the nucleophilic water and highlights residues near the catalytic zinc likely to be involved in recognition and catalysis of polymeric RNA substrates. A minimal 19 nucleotide RNA stem substrate has permitted the first steady-state kinetic characterization of this enzyme ($k_{cat} = 13 \pm 1$ min^{-1} and $K_M = 0.83 \pm 0.22$ μM). A continuous coupled assay was developed to follow the reaction at high concentrations of polynucleotide substrates (>10 μM). This work begins to define the chemical and structural determinants responsible for catalysis and substrate recognition and lays the foundation for detailed mechanistic analysis of this essential enzyme.

The conversion of genetically encoded adenosine (A) to inosine (I) at the wobble (5′-most) position 34 of tRNA anticodons is essential for the flow of biological information. This modification allows for a single tRNA species to recognize multiple synonymous codons containing A, C, or U in the last (3′-most) position, ensuring that each sense codon is appropriately decoded and provides an element of economy by reducing the number of required tRNA isoacceptors. Inosine at the wobble position of tRNA anticodons was first discovered in yeast tRNA^{Ala} (*1*) and has subsequently been found in eight eukaryotic tRNAs (seven in yeast). In the majority of eubacteria and plant chloroplasts, only a single species, tRNA^{Arg2}, is modified (*2*). The first experimental evidence of the enzyme-catalyzed conversion of A → I at the wobble position of the anticodon in eukaryotic tRNAs was obtained from the action of *Xenopus* extracts on the primary transcript of silkworm tRNA^{Ala} (*3*). A similar activity was shown to catalyze the direct hydrolytic deamination of all seven tRNAs in *Saccharomyces cerevisiae* (*4*).

The above activities are representative of the family of adenosine deaminases of tRNA (ADATs)[1] that specifically target the tRNA anticodon loop (*5*). Despite supporting the specific deamination of adenosine, sequence analysis demonstrates that the ADATs belong to the cytidine deaminase superfamily. Tad1p, the product of the *S. cerevisiae ADAT1* gene, catalyzes the modification of A37 → I37 in tRNA^{Ala}, where inosine is subsequently methylated by an unknown enzyme. Tad2p and Tad3p form a heterodimeric complex that specifically catalyzes the deamination of A34 → I34 (*6*). The central importance of this enzyme in the generation of I at position 34 is demonstrated by the observation that Tad2p and Tad3p are essential for viability, whereas Tad1p is not. The cloning and purification of the first prokaryotic ADAT, *E. coli* TadA (ecTadA), was recently reported (*7*). This enzyme exclusively catalyzes the deamination of A34 → I34 in tRNA^{Arg2}, the full length physiological substrate, as well as a ∼20 nucleotide minimized substrate composed of only the anticodon stem-loop sequence (Figure 1). These studies further suggested that the nucleotides at positions 33−36 provide major determinants for ecTadA substrate specificity. Notably, ecTadA was also shown to be an essential gene (*7*).

At present, detailed structure−function relationships for the ADATs have not been described due to the lack of both a high-resolution structure and a robust continuous assay. We report the crystal structure of ecTadA at 2.0 Å resolution

[1] Abbreviations: TadA, tRNA-specific adenosine deaminase; ADAT, adenosine deaminase acting on tRNA; GDH, glutamate dehydrogenase; TLC, thin-layer chromatography.

FIGURE 1: Reaction catalyzed by ecTadA. (A) ecTadA specifically modifies A34 of tRNA^{Arg2} in *E. coli*. The anticodon is highlighted in red. (B) The minimized stem loop utilized in the assay of ecTadA activity.
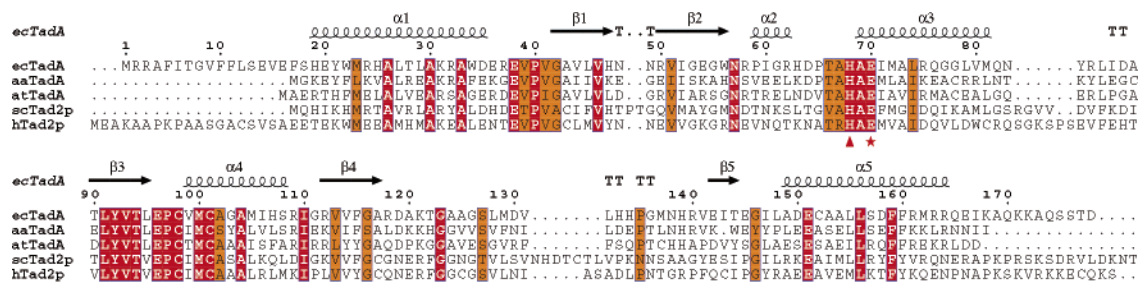

FIGURE 2: Multiple sequence alignment of tRNA-specific adenosine deaminase from *E. coli* (NCBI accession code P68398), *A. tumefaciens* (AAL41704), *A. aeolicus* (O67050), *S. serevisiae* (P47058), and human (CAD94290); numbering is based on the *E. coli* enzyme. The last 71 amino acids of scTad2p were omitted for clarity of presentation. The highly conserved residues are boxed in orange, and invariant residues are in red. The metal binding residues are marked by a red triangle, and the catalytic residue Glu70 is indicated by a red star. The schematic secondary structure of ecTadA is depicted on the top of the sequence alignments.

and a quantitative initial rate analysis with a truncated RNA stem-loop substrate. In addition, a continuous assay employing the glutamate dehydrogenase coupling system was developed and validated. This continuous assay is especially valuable in assaying deaminase activity with modified tRNA substrates that cannot be generated with T7 RNA polymerase. These studies reveal a tight dimeric structure for ecTadA, describe the disposition of the zinc-containing active site, and provide the first quantitative steady-state kinetic analysis for a bacterial member of the ADAT family.

MATERIALS AND METHODS

Expression and Purification. The full-length *E. coli* TadA (NCBI accession code P68398) was not soluble when expressed without an affinity tag or as a GST-fusion protein. As the ecTadA possesses an N-terminal extension not present in other bacterial homologues (Figure 2), a shorter sequence representing residues 13−178 of ecTadA was cloned into the *NdeI/XhoI* sites of pET30a, which supports the expression of untagged protein.

E. coli BL21 (DE3) cells were transformed with the expression vector coding for the N-terminally truncated ecTadA protein, grown in LB containing 50 μg/mL kanamycin at 37 °C until the OD$_{600}$ reached approximately 1, and induced with 0.4 mM IPTG. Growth was continued at 25 °C for 12 h, and the cells were harvested by centrifugation, resuspended in buffer (50 mM Tris-HCl, pH 8.0), and lysed by sonication on ice. After centrifugation at 27 000g for 1 h, the supernatant was applied to a MonoQ column (Amersham) and eluted with a linear gradient of NaCl, and appropriate fractions were applied to a Superdex75 column (Amersham). Final purity was over 95% as verified by SDS−PAGE analysis. Typical yields were 1.5 mg of untagged

ecTadA/L. Enzyme concentration was determined spectro-photometrically ($\epsilon_{280} = 1.18$ (cm^{-1} mL)/mg).

Synthesis of tRNA Stem-Loop Substrate. Construction of the tRNA stem loop was performed with the MEGAshort script T7 kit (Ambion). To incorporate radiolabeled adenosine, 3.5 μM [α -^{32}P]ATP (Amersham) was added to 0.25 mM unlabeled ATP in the T7 transcription mixture, which contains 1 μM T7 primer, 1 μM antisense DNA template, and 3.75 mM CTP, UTP, and GTP. The reaction was carried out overnight at 37 °C. The RNA was purified by electro-phoresis on an 8 M urea polyacrylamide gel eluted with 0.5 M ammonium acetate, 0.2% SDS, and 1 mM EDTA; and ethanol precipitation. The RNA was resuspended with RNase-free water, and the OD$_{260}$ was measured for quantitation.

Kinetic Assay of ecTadA. The deamination activity of ecTadA with a 19 base pair RNA stem loop was assayed as described previously with modifications (*7*). The reaction was initiated by addition of ecTadA to the assay solution including 10 mM Tris-HCl, pH 8.0, and varying concentrations of RNA substrates at 25 °C. The concentration of ecTadA used in the assay was adjusted to achieve steady-state rates (0.25−2.5 nM). An aliquot of the assay solution was removed periodically and quenched with 250 mM MES (pH 5.0) buffer which had been preheated to 70 °C. P1 nuclease (US Biological) was added and incubated at 70 °C for 1 h before spotting on cellulose thin-layer chromatography (TLC). The monophosphates were separated by TLC with a buffer containing 3 M (NH$_4$)$_2$SO$_4$/0.1 M NaOAc (pH 6.0)/2-propanol (79:19:2, (v/v/v)) (*8*). Images of the radioactive TLC were recorded on a phosphorimaging plate (Molecular Dynamics) and analyzed using a Molecular Dynamics Storm 860 PhosphorImager System with ImageQuant software. Kinetic constants were derived by fitting the experimental data to eq 1 using Sigma Plot, where v is the rate of

the reaction, E_T is the total concentration of ecTadA, k_{cat} is the maximal velocity, K_m is the Michaelis constant, and S is the substrate concentration

$$\nu/E_T = k_{cat}S/(K_m + S) \qquad (1)$$

A continuous coupled assay was developed to follow the initial steady-state rates of ecTadA at high concentrations of polynucleotide substrates ($>10\ \mu M$), including the tRNA^{Arg2} anticodon stem loop, the product stem loop, and the 2′-deoxy stem-loop analogue. The deamination of adenosine to inosine was measured by coupling ammonia release to the glutamate dehydrogenase (GDH)-catalyzed reductive amination of α-ketoglutarate, which conveniently allows the oxidation of NADPH to be monitored at 340 nm as a function of time (*9, 10*). Unlabeled RNA stem-loop substrates were purchased from Dharmacon. The assay solution includes 100 mM Tris-HCl, pH 8.0, 5 mM α-ketoglutarate, 0.2 mM NADPH, 3 units of GDH, and varying amounts of substrates in 100 μL. The assay was performed at 25 °C.

Analytical Ultracentrifugation Experiments. Sedimentation velocity experiments were performed with a Beckman Optima XL-I centrifuge using a Ti 60 rotor at 25 °C. Protein samples contained 0.27, 0.54, or 0.88 mg/mL of ecTadA in 50 mM Tris-HCl, pH 8.0, and 100 mM KCl. The 12 mm double sector aluminum centerpieces were used with a sample capacity of 400 μL. All experiments were conducted at a rotor speed of 42 000 rpm (125 000*g*), and scans were taken for 2 h. The sedimentation of ecTadA was monitored by the absorption of light at 280 nm. The sedimentation data were analyzed with the computer program SVEDBERG (*11*).

Crystallization and Structure Determination. Diffraction quality crystals were obtained by hanging drop vapor diffusion at 21 °C by mixing 1 μL of ecTadA (11 mg/mL) with 1 μL of reservoir solution containing 0.1 M sodium chloride, 0.1 M Bicine, pH 9.0, and 20% (v/v) poly(ethylene glycol) monomethyl ether 550, and equilibrating samples against reservoir solution for 3 weeks. Diffraction from these crystals is consistent with the space group $I4_122$ with unit cell dimensions a = b = 100.2 Å, c = 159.6 Å, and two ecTadA molecules in the asymmetric unit.

A single crystal of ecTadA was briefly transferred to reservoir solution containing 15% glycerol and flash-cooled in a nitrogen stream at 100 K (Oxford Cryosystems, Oxford, U.K.). Diffraction data were collected to 2.03 Å resolution at the X29A beamline (National Synchrotron Light Source) using a Quantum 315 CCD detector (Area Detector Systems Corporation, Poway, CA). The intensities were integrated with HKL2000 (*12*) and reduced to amplitudes using TRUNCATE (*13*) (Table 1). The structure of ecTadA was solved with the molecular replacement program PHASER (*14*), using a partial polyserine model constructed with SWISS-MODEL (*15*). Two unique rotation−translation solutions were identified, suggesting that two ecTadA chains form a tightly associated dimer with the molecular two-fold axis oriented diagonally within the crystal *xy*-plane. The partial dimer model was refined with CNS1.1 (*16*) and passed to the autobuilding algorithm in Arp/wArp (*17*). Fifty cycles of autobuilding and refinement with Refmac (*13*) produced a model that accounted for 85% of the sequence and yielded an excellent electron density map that allowed manual

Table 1: Data Collection and Refinement Statistics

Data Collection	
Resolution, Å	30.0−2.03
Observed reflections	189 859
Unique reflections	26 559
Completeness, (40%)	100.0 (100.0)^a
$R_{merge}{}^b$	0.075 (0.485)^a
Refinement	
Protein nonhydrogen atoms	2458
Water molecules	226
$R_{cryst}{}^c$	0.176 (0.223)^a
$R_{free}{}^c$	0.216 (0.287)^a
Average B-factor, (Å^2)	33.1
Main chain	29.7
Side chains	36.6
Waters	46.7
rmsd from ideal geometry	
Bond length, Å	0.016
Bond angles, (deg)	1.7
Torsion angles, (deg)	23.1

^{a} Values in parentheses correspond to highest resolution shell 2.10−2.03 Å. ^{b} $R_{merge} = \sum\sum_j |Ij(hkl) - \langle I(hkl)\rangle|/\sum\sum_j |\langle I(hkl)\rangle|$, where Ij is the intensity measurement for reflection j and $\langle I \rangle$ is the mean intensity over j reflections. ^{c} $R_{cryst}/(R_{free}) = \sum ||F_{obs}(hkl)| - |F_{calc}(hkl)||/\sum|F_{obs}(hkl)|$, where F_{obs} and F_{calc} are observed and calculated structure factors, respectively. No σ-cutoff was applied. Five percent of the reflections were excluded from refinement and used to calculate R_{free}.

building of the remaining residues and solvent molecules (R_{cryst} and R_{free} of 0.176 and 0.216, respectively). A single strong peak of electron density ($\sim 9\sigma$) within each subunit was initially fit as a water molecule. However, an abnormally low-temperature factor (2.0 Å^2 compared to the average 21.2 Å^2 for neighboring groups), characteristic tetrahedral coordination, and interatomic distances suggested the presence of a bound Zn^{2+} ion. With this assignment, the individual temperature factors of the ions refine to 20.5/21.4 Å^2, well in accordance with the values for the surrounding groups. Visual analysis and model manipulations were performed with the program O (*18*). The quality of the final structure was verified with the composite omit maps, and the stereochemistry was checked with the program PROCHECK (*19*). All residues were found in the allowed region of the Ramachandran plot (86.4% in the most favored and 13.6% in the additional allowed). Figures were produced with O (*17*), PyMOL (DeLano Scientific, LLC), Swiss-PdbViewer (http://www.expasy.org/spdbv/), and POVRAY (http://www.povray.org).

RESULTS

Purification and Characterization of ecTadA. The full-length protein exhibited poor solubility; however, removal of residues 2−12 yielded soluble material. Size exclusion and anion exchange chromatography yielded 1.5 mg of homogeneous protein per liter of *E. coli* fermentation (Figure S1 in Supporting Information). ecTadA eluted from a Superdex75 (Amersham) size exclusion column between ovalbumin (MW = 43 kDa) and chymotrypsinogen A (MW = 25 kDa). Sedimentation velocity experiments with ecTadA yielded $s_{20,w}$ of 3.4, 3.3, and 3.0 S at concentrations of 0.27, 0.54, and 0.88 mg/mL, respectively. This behavior indicates that the recombinant protein forms a dimer in solution, consistent with previous data (*7*).

Kinetic Assay. The activity of the truncated protein was assayed with a minimized anticodon stem-loop sequence of
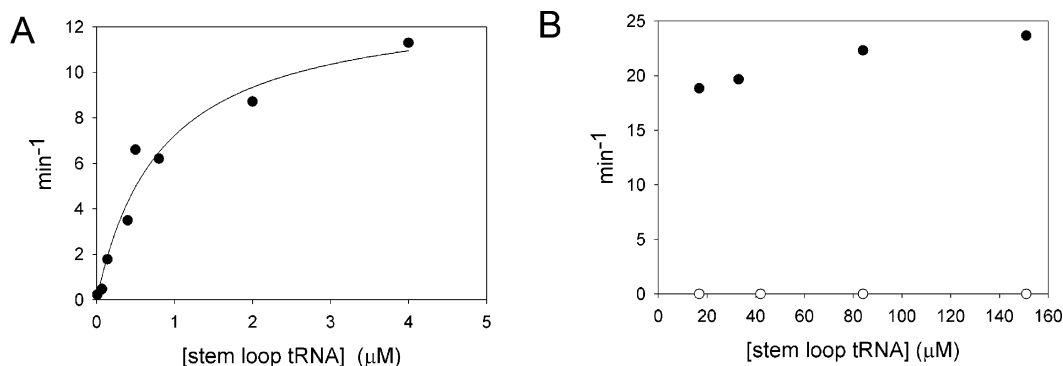
FIGURE 3: (A) Michaelis–Menten plot of an initial rate assay on the ^{32}P-labeled stem loop tRNA[arg2]. The concentration of the substrate used in the assay varies from 10 nM to 4.0 μM. (B) An initial rate measurement on the stem loop tRNA[arg2] (●) or the product stem loop (○) using glutamate dehydrogenase-coupled system.

tRNA[Arg2], previously reported to be a substrate for ecTadA (Figure 1) (*7*). The kinetic parameters of the reaction were determined under steady-state conditions using a ^{32}P-labeled RNA generated by T7 runoff, where the concentration of the substrate ranges from 10 nM to 4.0 μM: $k_{cat} = 13 \pm 1$ min[−1] and $K_M = 0.83 \pm 0.22$ μM (Figure 3 and Figure S2 in Supporting Information). The activity was also measured with a glutamate dehydrogenase coupling system. Because of the low extinction coefficient of NADPH, rates could only be measured at substrate concentrations exceeding 10 μM. As expected from the K_M determined from the TLC-based assay, rates were essentially constant ($\sim$20 min^{−1}) over a stem-loop RNA concentration of 16−150 μM. The *product stem loop*, which contains inosine instead of adenosine at the wobble position, yielded no detectable activity at concentrations to 150 μM, confirming that deamination occurs specifically at A34 (Figure 3). A stem-loop sequence composed of 2′-deoxynucleotides did not exhibit any activity as either a substrate or an inhibitor at concentrations up to 150 μM. Adenine, adenosine, and adenine nucleotides also did not serve as substrates.

Overall Structure of the ecTadA Dimer. Most of the ecTadA construct (residues 13−178) is well-defined in the electron density maps, except for the first two N-terminal residues of the construct and the last 10 C-terminal residues, which are not included in the model. Each monomer consists of a central five-stranded β-sheet (strands β1−β5), flanked by two α-helices (α1,α5) on one side, and by three α-helices (α2−α4) on the opposite side. Two independent ecTadA molecules are present in the asymmetric unit and form a substantial interface with total surface area and total buried surface area of 14 110 and 2860 Å[2], respectively, as calculated with AREAMOL (Figures 4A and 5) (*13*). This organization is consistent with gel filtration and sedimentation analyses (see above), indicating that ecTadA is a homodimer in solution. Each monomer contributes 14 polar and 19 nonpolar residues to the dimer interface with only two symmetry-related hydrogen bonds formed between Asp64 O$_{\delta2}$ of one subunit and Arg75 N$_\epsilon$ of the second subunit (3.3/2.9 Å, respectively). The Asp64Glu mutant of ecTadA is fully active in vivo, but not in vitro, indicating that this area might be involved in important protein−protein interactions (*7*). Of the 33 interfacial residues, six are strictly conserved within the ADAT family and only two, His68 and Cys98, are conserved within the greater cytidine deaminase

superfamily, consistent with their role in coordinating the catalytically essential Zn^{2+} ion (Figure 2).

DISCUSSION

ADATs belong to the cytidine deaminase superfamily, which includes cytidine deaminase, guanine deaminase, and RNA/DNA editing enzymes (*20−24*). The crystal structures of cytidine deaminases from *Bacillus subtilis* and *E. coli* and of guanine deaminase from *B. subtilis* have been reported, and all exhibit a similar overall fold and active site architecture (*22*). The active sites of these enzymes contain a tetrahedrally coordinated zinc ion, with two cysteine and a single histidine ligands contributed from the protein. The fourth ligand is provided by solvent and is the catalytic water nucleophile. A virtually identical arrangement is observed in ecTadA and suggests a similar mechanism for deamination. The activated zinc-bound water is hydrogen-bonded to Glu70 and is thereby activated for attack on C_6 of the purine ring to yield a tetrahedral intermediate. The subsequent elimination of ammonia requires protonation of the amino group prior to elimination. Solvent water or Glu 70 could provide the proton (Figure 6). Glu 70 is positioned to transfer a proton between the Zn-bound water, the amino group of adenosine, the covalent intermediate and possibly solvent water. The distance between the catalytic water and zinc (2.11/1.98 Å) is consistent with either bound water (Zn−OH$_2$) or hydroxide (Zn−OH) and the Glu 70 serving in an acid/base capacity for the required proton transfer.

Kinetic Properties of ecTadA. The N-terminally truncated protein was shown to be active in deamination of the anticodon stem loop from tRNA[Arg2] using a traditional ^{32}P-based TLC assay ($k_{cat} = 13 \pm 1$ min[−1], $K_M = 0.83 \pm 0.22$ μM). The recombinant enzyme is active without the addition of exogenous zinc ion; as supported by the X-ray structure, the tightly bound and catalytically essential zinc remains associated during purification. The kinetic properties of mammalian adenosine deaminase are well-characterized, with the k_{cat} and K_M of 188 s^{−1} and 33 μM, respectively (*25*). The k_{cat} and K_M for *E. coli* cytidine deaminase are 299 s^{−1} and 120 μM, respectively (*26*). Despite the high k_{cat} values of these deaminases, *E. coli* TadA has a k_{cat}/K_M of 2.6 × 10^{5}, within a factor of 20 of adenosine and cytidine deaminases. There are relatively limited reports on the kinetic characterization of the polynucleotide modifying deaminases. Tad1p from *Drosophila melanogaster* catalyzes the deamination from A37 within the anticodon loop of tRNA[Ala] at
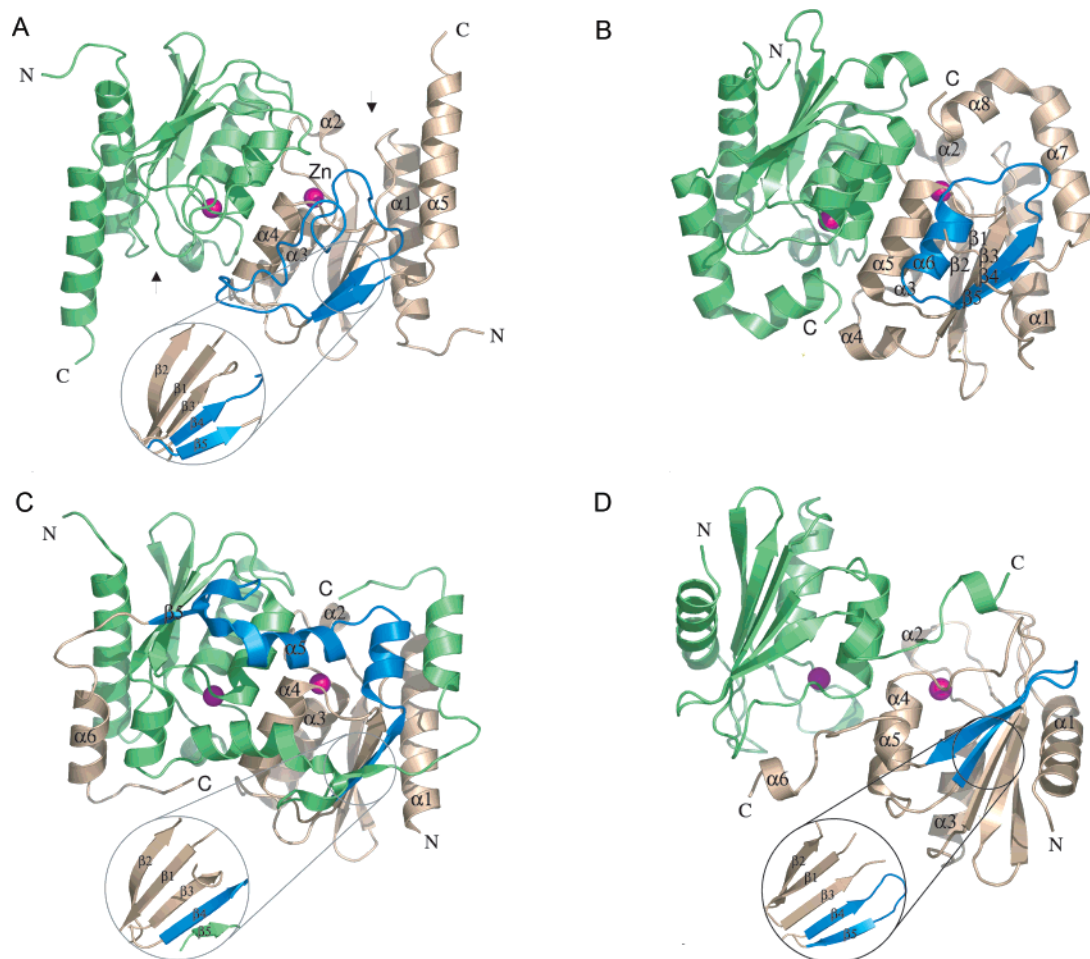
FIGURE 4: Oligomerization modes in ecTadA and related deaminases. Pink spheres denote active site zinc ions. (A) Overall architecture of the ecTadA dimer. The $\beta4$-$\beta5$ loop is in blue. The subunit interface is extensive, predominantly nonpolar, and includes both active sites. Interactions between the N-terminal ends of the zinc-binding helices $\alpha4$ are crucial. Active sites entrances are indicated by arrows. (B) The dimerization mode in yeast cytosine deaminase (1P6O) is similar except for the relative parallel shift of the helices $\alpha5$ (equivalent to $\alpha4$ in ecTadA) (*29*). C-terminal parts of each chain (helix $\alpha8$) partially block the active site entrances. β-Sheet topology is identical to ecTadA. (C) In *B. subtilis* guanosine deaminase (1WKQ), the subunit interface is relatively larger that in other deaminases due to the C-terminal domains swap. (D) *B. subtilis* cytidine deaminase (1JTK, shown) and yeast RNA-specific cytidine deaminase (1R5T) form tightly bound tetramers. However, subunits A and B (or C and D) also dimerize through helices $\alpha4$, similarly to the dimeric deaminases. Note different orientation of $\beta5$ within the β-sheet.

6.7 min^{-1} (*27*). The yeast Tad1p has been assayed with tRNA^{Ala} from *S. cerevisiae*, which yielded the kinetic constants of $k_{cat} = 4.2$ min^{-1} and $K_M = 6 \pm 4$ nM (*5*). A partially purified tRNA A34 deaminase from yeast exhibited $K_M = 2.3 \pm 0.4$ nM when assayed with the yeast tRNA^{Ser} (*4*). The relatively high K_M for ecTadA compared to other ADATs could be the consequence of the truncation of the N-terminus in the recombinant enzyme, though this possibility is considered unlikely given the considerable sequence divergence present in this region of the TadA homologues (Figure 2). Alternatively, these differences might be due to the use a minimized stem-loop substrate, which could be detrimental due to the removal of recognition determinants present in the full-length substrate and/or decreased stability of the stem-loop structure relative to the intact tRNA. Finally, the differences could represent different catalytic capacities for the bacterial and eukaryotic enzymes. The much higher k_{cat} and K_M of the metabolic deaminases might reflect the higher in vivo abundance of single nucleotide species and the need for high fluxes through these pathways to support overall cell physiology.

We also developed a continuous coupled assay for ecTadA; unfortunately, this assay did not allow for the rates to be determined below micromolar substrate concentration due to the detection limit of the spectroscopic method. However, the rate at saturating substrate is similar to the turnover number (k_{cat}) derived from the conventional TLC-based assay with ^{32}P-labeled substrate (Figure 3). Therefore, k_{cat} can be measured conveniently using the isotope-free, continuous assay system. This continuous assay will find applications in other systems catalyzing the deamination of polynucleotides and will allow for the use of polynucleotide substrates containing modifications that are not compatible with the T7 transcription system (e.g., RNA$-$DNA chimeras and substrate-containing modified bases).

EcTadA was tested for activity with various substrates in addition to the anticodon stem loop of tRNA^{Arg2}, including the 2′-deoxy stem loop, adenine, adenosine, AMP, ADP, and ATP. Only the stem-loop RNA proved to be a substrate for ecTadA, demonstrating a high specificity. In a previous report, it was demonstrated that the stem-loop structure containing the anticodon loop sequences is sufficient for
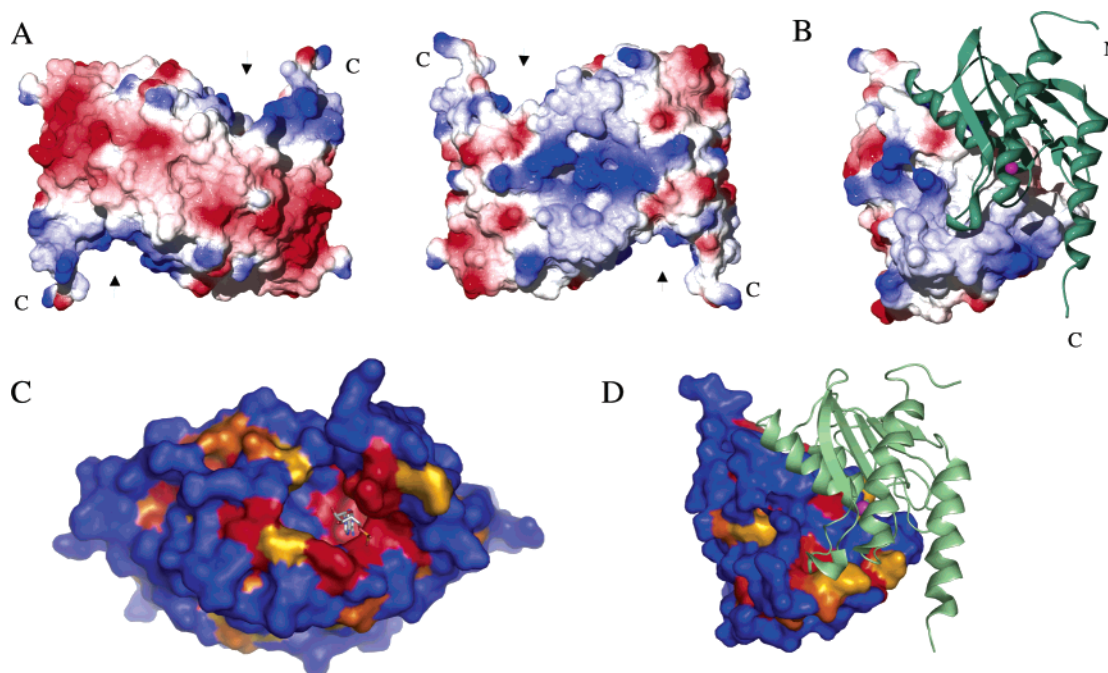
FIGURE 5: The molecular surface presentation of ecTadA. (A) The areas of positive electrostatic potential (blue, $+3kT$/e) are concentrated in and around the active sites (indicated by arrows) and on the front side of the molecule (right panel) around the molecular two-fold axis. The extended areas of negative potential (red, $-3kT$/e) are concentrated on the opposing tips of the front side of the molecule and run across most of the central part of the opposite side. (B) One subunit of the dimer is presented as molecular surface, and the other subunit is shown as ribbon. The subunit interface is much less polar than the solvent accessible areas. (C) The molecular surface, with the molecule rotated 90° about a horizontal axis relative to panel A, colored according to the amino acid sequence conservation within TadA family: red, invariant; orange, conserved; blue, not conserved. The modeled position of A34 within the active site is shown. The highest sequence conservation occurs in the core of the molecule and around the active site entrance. (D) The sequence conservation at the subunit interface is only partial.
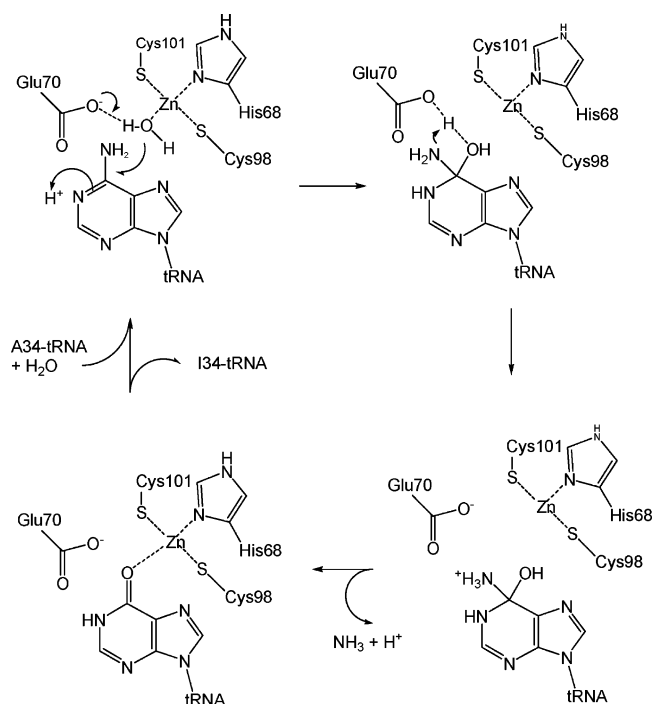

FIGURE 6: Proposed mechanism of deamination by ecTadA.

deamination by ecTadA (*7*). Nucleotides outside the anticodon region may interact with the enzyme to facilitate binding and presentation of A34 to the zinc-bound active site; however, these determinants cannot be directly identified from the ligand-free ecTadA structure.

The minimized anticodon stem loop of tRNA^{Arg2} contains three adenosines besides A34, two in the stem region and one within the anticodon loop region. The deamination of this substrate occurs exclusively at A34, since no activity was observed with the product stem loop containing I at position 34. It is notable that 2′-deoxyoligos did not function as either a substrate or an inhibitor for ecTadA. By analogy with other systems, the binding of 2′-deoxyoligos might have been compromised by the absence of specific interatomic interactions, as has been demonstrated with tRNA^{Ala} synthetase, where dG4-, dC71-, and dU70-containing RNA substrates were charged less efficiently than substrates with 2′-deoxy modifications at other positions (*28*). Alternatively, it is possible that the lack of interaction is the consequence of overall structural differences between RNA and DNA polymers (e.g., interphosphate distances and differences in major and minor groove properties).

Structural Comparisons in the Cytidine Deaminase Superfamily. The structure of ecTadA places it within the cytidine deaminase superfamily, and analysis of the structurally characterized members reveals three different modes of oligomerization: (i) dimeric without domain swap, as in the current structure and yeast cytosine deaminase (*21, 29*) (Figures 4A,B); (ii) dimeric with domain swap, as in *B. subtilis* guanine deaminase (*22*) (Figure 4C); and (iii) tetrameric with partial domain swap, as in yeast RNA-specific cytidine deaminase (*30*) and *B. subtilis* cytidine deaminase (*31*) (Figure 4D). The major topological differences in these otherwise similarly folded proteins occur at the C-terminus of β-strand β4. In the enzymes of the first group, β4 is followed by a long loop segment (residues Gly106−Asn128 in ecTadA) that allows β5 to pack against β4 in a parallel mode. In the second group, this long loop
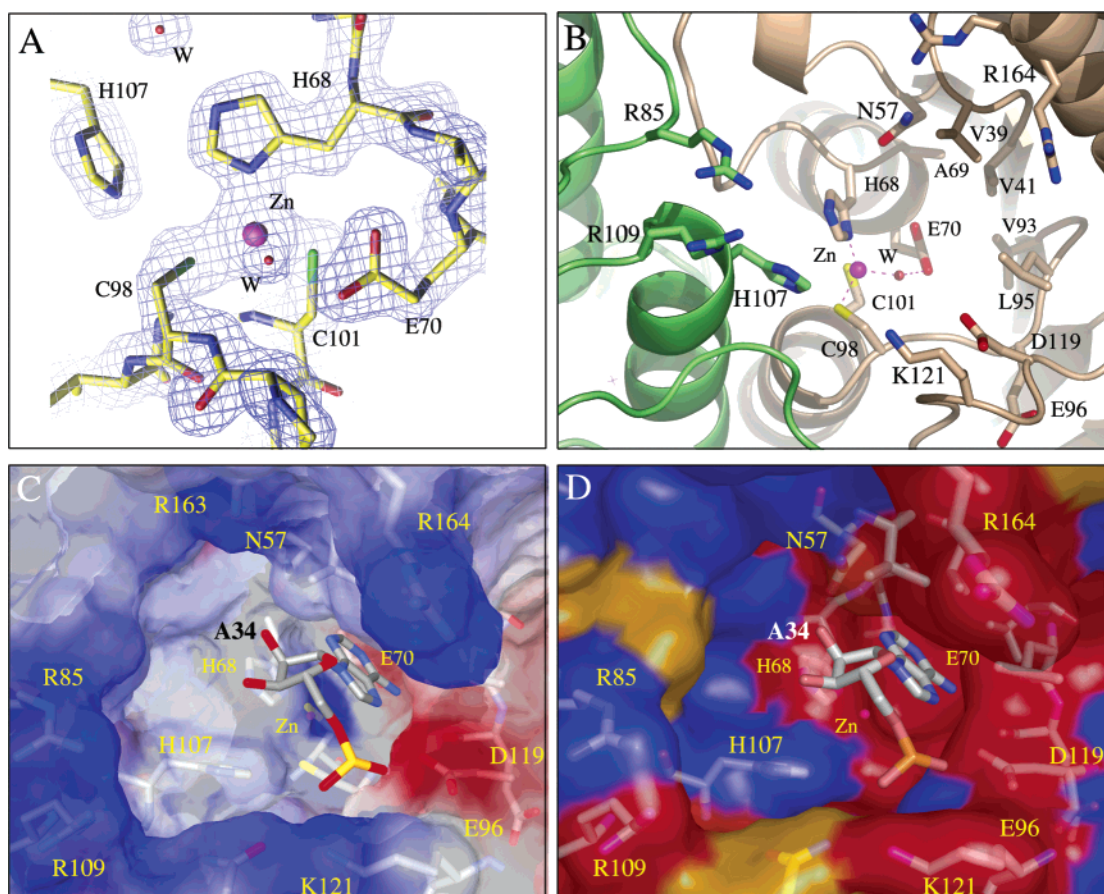
FIGURE 7: The active site of ecTadA. (A) Experimental $(2F_o - F_c)$ electron density map. Pink and red spheres represent zinc (Zn) and water (W), respectively. (B) The detailed view of the active site from the entrance (similar orientation as in Figure 5C). The active site is composed of residues of both subunits (shown in different colors). Residues thought to be involved in catalysis and tRNA^{Arg2} binding are indicated. (C) Molecular surface representation of the active site entrance (same orientation as in panel B). Patches of positive electrostatic potential (blue) surrounding the entrance might be important for positioning of the negatively charged substrate within the active site. The modeled position of tRNA^{Arg2} A34 is based on the inhibitor-bound structures of yeast cytosine deaminase (1P6O) and *E. coli* cytidine deaminase (1AF2). (D) The same as panel C, but the molecular surface is colored according to the sequence conservation (see Figure 5C,D).

segment allows $\beta5$ to pack in the same parallel mode against $\beta4$ of the second subunit, bringing helix $\alpha6$ all the way across the second subunit in close contact with its N-terminal $\alpha1$. In the third group, the loop between $\beta4$ and $\beta5$ is relatively short, promoting an antiparallel interaction that bridges the short C-terminal helix into contact with the second subunit. Dissociation into dimers is unlikely, as both intradimer and interdimer interfaces within the tetramer are extensive and likely to contribute to the overall stability of the tetrameric species. The larger *E. coli* cytidine deaminase is unique, as it possess an additional N-terminal domain containing three α-helices, an additional C-terminal domain containing a four-stranded β-sheet, and three α-helices, and adds a sixth β-strand to the central β-sheet. On the basis of the mode of dimerization, *E. coli* cytidine deaminase can be attributed to the first group, but the β-strands equivalent to $\beta4$ and $\beta5$ pack in an antiparallel manner as in tetrameric deaminases (i.e., yeast RNA-specific and *B. subtilis* cytidine deaminases).

Despite significant topological differences, the members of all three groups show remarkably similar features with dimer formation occurring primarily through the N-terminal ends of helix $\alpha4$ ($\alpha5$ in yeast cytosine deaminase), which bears the highly conserved zinc-binding motif P-C-x−x-C (Figures 4). Notably, the distance between the zinc atoms of two subunits remains within the range of 13.9 (in the current structure) to 14.7 Å (in *B. subtilis* cytidine deaminase) for the other members of cytidine deaminase superfamily with known structures. The actual role of oligomerization in substrate selection is yet to be fully understood.

Active site and Mechanistic Features of ecTadA. Hydrolases commonly utilize catalytic site zinc to polarize or ionize water toward a highly nucleophilic hydroxyl ion. The ions in both ecTadA subunits display tetrahedral coordination with His68 $N_{\delta1}$ (2.01/2.01 Å), Cys98 S_γ (2.24/2.37 Å), Cys101 S_γ (2.27/2.24 Å), and a water molecule (2.11/1.98 Å) serving as ligands (Figure 7A,B). These residues are highly conserved within the cytidine deaminase superfamily. Interestingly, the mammalian adenosine deaminases (e.g., PDB codes: 2ADA and 1NDW (*32, 33*)), which catalyze the hydrolysis of free adenosine, are monomeric $\alpha−\beta$ barrel proteins. In these enzymes, the Zn ion is tetrahedrally coordinated, with three histidines and a water molecule serving as ligands.

In ecTadA, the presumptive catalytic site appears as an elongated groove, which narrows dramatically near the zinc ion, such that only a single nucleotide can be accommodated in the absence of a substantial structural reorganization (Figures 5C and 7C,D). This constraint suggests that alterations in phosphodiester backbone torsion angles must occur upon association with TadA. It is possible that A34

"flips out" from the anticodon stem loop to provide appropriate steric features for recognition and catalysis. Base flipping is well-documented in a number of polymeric nucleic acid modifying enzymes, including methyl transferases and glycosylases, as an essential mechanistic element for the presentation of the target base to the catalytic site. In addition to alterations in the phosphodiester backbone, flipping is associated with the disruption of π-stacking interactions between adjacent bases in nucleic acid polymers. The importance of π-stacking interactions for the structure and function of globular nucleic acids is highlighted by its prevalence in tRNAs. For example, in the structure of the yeast tRNA^{Phe}, 42 of the 76 residues participate in interbase hydrogen bonding interactions (e.g., Watson–Crick, Hoogsteen, etc.), while 71 of the bases participate in π-stacking interactions (*34–36*). It is notable that stacking interactions are observed not only in double-stranded regions, but also in single-stranded regions including residues 34–38 in the anticodon loop. This feature may be of particular mechanistic importance to the TadA homologues , as the placement of A34 (i.e., the wobble position in *E. coli* tRNA^{Arg2}) at the beginning of a run of single-stranded stacked nucleotides (e.g., stacking with only residue 35) imposes fewer energetic constraints on this nucleotide than those involved in stacking interaction on both sides and may facilitate flipping and presentation of A34 to the ecTadA catalytic site.

The walls of the active site groove have extended patches of positive electrostatic potential to interact with the tRNA^{Arg2} phosphate backbone and properly orient the RNA within the active site. As previously noted, the C-terminal helix α5 seems to be an important tRNA anchor bearing a conserved FFxxxR motif (*37*). Among basic residues lining the active site entrance are Lys121, Arg163, Arg164, and the residues from the neighboring subunit, Arg85, His107, and Arg109. The contribution of residues from both subunits for substrate recognition highlights the importance of the dimeric organization for TadA function.

To identify potential binding determinants for the recognition and hydrolysis of A34 in tRNA^{Arg2}, a model of the enzyme–substrate complex was generated based on the homologous structures of the yeast cytosine deaminase bound to the inhibitor 4-hydroxy-3,4-dihydro-1h-pyrimidin-2-one (*29*) and *E. coli* cytidine deaminase bound to uridine (*38*). The active sites of both structures fit well with the active site of ecTadA, and the positions of the inhibitors are similar. On the basis of the previously determined structures of the members of this family, Glu70 was proposed to activate the zinc-bound water molecule and facilitate nucleophilic attack on the C$_6$ atom of the adenine residue. In our model (Figures 6 and 7C,D), the adenine ring is proposed to stack on the imidazole ring of His68, which is also involved in zinc coordination, and the N$_6$ atom of A34 is appropriately positioned for nucleophilic attack by the activated water molecule. This binding mode of A34 would be stabilized by potential hydrogen bonds between adenine heteroatoms and neighboring protein functionalities, including main chain atoms of Glu96 and Cys98 and the side chains of Asn57 and Glu70. A number of nonpolar residues, including Val39, Val41, Leu95, Pro97, and Phe160 provide important van der Waals contacts to the ribose and purine base of A34. Importantly, all of the above residues are highly conserved among the bacterial wobble-specific deaminases. It is notable

that, in the absence of substrate, the A34-binding pocket is occupied by six water molecules that recapitulate many of the potential hydrogen bonds between A34 and the conserved polar atoms in the pocket. Similar water clusters are also present in the TadA structures from *Aquifex aeolicus* and *Agrobacterium tumefaciens* (*37, 39*).

Notably, the anticodon stem loop of tRNA^{Arg3} which contains the anticodon of CCG is not deaminated by ecTadA (i.e., there was no conversion of C → U and ammonia); however, deamination was observed when this cytidine was replaced with adenine (*7*). Our structural model suggests a partial explanation for this observation: due to the difference in steric properties between purines and pyrimidines, if cytidine in position 34 is oriented productively within the active site, unfavorable steric interactions between the nucleic acid backbone and ecTadA would result.

Comparison with Other TadA Structures. The crystal structures of TadAs from *A. aeolicus* (aaTadA) and *A. tumefaciens* (atTadA) have recently been reported (*37, 39*). These proteins exhibit ∼35% sequence identity with the ecTadA. The overall folds of all three enzymes, and especially the architectures of the metal binding sites, are highly similar. The overall rmsd values between the C$_\alpha$ atoms of the ecTadA monomer and those of aaTadA and atTadA are 0.95 and 1.1 Å, respectively, whereas for the active site residues (within 10 Å radius from the Zn ion), rmsd values are 0.33 and 0.30 Å, respectively. As expected, the highest sequence conservation occurs around the active site and at the subunit interface.

Of particular note is the C-terminal helix (α5), which adopts a similar conformation in both the aaTadA and ecTadA crystal structures. Interestingly, the atTadA structure lacks the last two turns of this helix, as the consequence of a proteolytic cleavage following the equivalent of ecTadA Phe159 that occurs during storage. The truncated atTadA protein exhibits 2000-fold less activity than wild-type, implying the significant role for α5 in catalysis (*37*), although, due to the utilization of a single endpoint assay, the effects on k_{cat} and K_m could not be determined. The placement of α5 in the ecTadA structure suggests a potential role in substrate binding (Figures 4A, 5A,C, and 7C,D). Kuratani et al. proposed a similar function for α5 in aaTadA, where two positively charged residues on α5 (residues 161 and 164 in *E. coli*) may stabilize the interactions with the negatively charged tRNA phosphates (*39*). Indeed, ecTadA and atTadA contain arginines in corresponding sites, although no such conservation is observed in the heterodimeric yeast or human enzymes (Figure 2).

Two highly conserved phenylalanines on α5 have been demonstrated to be important for catalysis by atTadA. Mutation of Phe144 (Phe159 in *E. coli*) to alanine reduced the enzymatic activity by 800-fold, while mutation of Phe145 (Phe160 in *E. coli*) to alanine completely abolished the activity (*38*). Again, the effects on k_{cat} and K_M were not examined. These two amino acids are located on the same side of the α5 in both ecTadA and aaTadA with the side chain oriented toward the hypothesized tRNA-binding cleft, suggesting a potential role in recognition of determinants on tRNA substrates distal from the site of chemistry. The equivalent of *E. coli* Phe160 is replaced with tyrosine in the catalytically active subunit (Tad2p) of the heterodimeric *S. cerevisiae* and human homologues (Figure 2).

On the basis of the proteolytic sensitivity of the atTadA and an analysis of α5 packing interactions in the atTadA crystals, it was suggested that the C-terminus of α5 may have intrinsic conformational plasticity (*39*). In the ecTadA structure, *B*-factors gradually increase toward the C-terminus of α5, exceeding the average overall *B*-factor (35.2 Å²) at Asp158, and the electron density completely disappears past residue Lys168. These data, taken in combination with the above mutagenesis data, suggest that α5 is indeed inherently dynamic and may undergo a modest disorder−order transition upon binding tRNA^Arg2.

In summary, we present the first combined structural and steady-state kinetic characterization of a wobble-specific tRNA adenosine deaminase. These studies define the structural and chemical determinants responsible for catalysis and substrate recognition and provide the foundation for a detailed mechanistic analysis of this essential enzyme.

NOTE ADDED IN PROOF

During the review of this paper, a paper describing the crystal structure of *Staphylococcus aureus* TadA complexed with an RNA stem-loop analogue was reported (*40*). This work supports the major mechanistic conclusions presented here.

ACKNOWLEDGMENT

SUPPORTING INFORMATION AVAILABLE

SDS−PAGE gel of the expression and the purification of ecTadA is shown in Figure S1; an example of the TLC of the time-resolved assay with ³²P-labeled RNA is shown in Figure S2. This material is available free of charge via the Internet at http://pubs.acs.org.

REFERENCES

1. Holley, R. W, Apgar, J., Everett, G. A., Madison, J. T., Marquisee, M., Merrill, S. H., Penswick, J. R., and Zamir, A. (1965) Structure of a ribonucleic acid, *Science 147*, 1462−1465.
2. Sprinzl, M., Horn, C., Brown, M., Ioudovitch, A., and Steinberg, S. (1998) Compilation of tRNA sequences and sequences of tRNA genes, *Nucleic Acids Res. 26*, 148−153.
3. Hagenbuchle, O., Larson, D., Hall, G. I., and Sprague, K. U. (1979) The primary transcription product of a silkworm alanine tRNA gene: identification of in vitro sites of initiation, termination and processing, *Cell 18*, 1217−1229.
4. Auxilien, S., Crain, P. F., Trewyn, R. W., and Grosjean, H. (1996) Mechanism, specificity and general properties of the yeast enzyme catalysing the formation of inosine 34 in the anticodon of transfer RNA, *J. Mol. Biol. 262*, 437−458.
5. Gerber, A., Grosjean, H., Melcher, T., and Keller, W. (1998) Tad1p, a yeast tRNA-specific adenosine deaminase, is related to the mammalian pre-mRNA editing enzymes ADAR1 and ADAR2, *EMBO J. 17*, 4780−4789.
6. Gerber, A. P., and Keller, W. (1999) An adenosine deaminase that generates inosine at the wobble position of tRNAs, *Science 286*, 1146−1149.
7. Wolf, J., Gerber, A. P., and Keller, W. (2002) tadA, an essential tRNA-specific adenosine deaminase from *Escherichia coli*, *EMBO J. 21*, 3841−3851.
8. Bass, B. L., and Weintraub, H. (1988) An unwinding activity that covalently modifies its double-stranded RNA substrate, *Cell 55*, 1089−1098.
9. Smith, E., Austin, B., Blumenthal, K., and Nyc, J. (1975) *The Enzymes*, pp 293−367, Academic Press, New York.
10. Bera, A. K., Smith, J. L., and Zalkin, H. (2000) Dual role for the glutamine phosphoribosylpyrophosphate amidotransferase ammonia channel. Interdomain signaling and intermediate channeling, *J. Biol. Chem. 275*, 7975−7979.
11. Philo, J. S. (1995) *Modern Analytical Ultracentrifugation*, Birkhauser, Boston, MA.
12. Otwinowski, Z., and Minor, W. (1997) Macromolecular crystallography, part A, in *Methods in Enzymology* (Carter, C. W., Jr., and Sweet, R. M., Eds.) pp 307−326, Academic Press, New York.
13. Collaborative Computational Project, No. 4 (1994) The CCP4 suite: programs for protein crystallography, *Acta Crystallogr. D. Biol. Crystallogr. 50*, 760−763.
14. Storoni, L. C., McCoy, A. J., and Read, R. J. (2004) Likelihood-enhanced fast rotation functions, *Acta Crystallogr., Sect. D: Biol. Crystallogr. 60*, 432−438.
15. Schwede, T., Kopp, J., Guex, N., and Peitsch, M. C. (2003) SWISS-MODEL: an automated protein homology-modeling server, *Nucleic Acids Res. 31*, 3381−3385.
16. Brunger, A. T., Adams, P. D., Clore, G. M., DeLano, W. L., Gros, P., Grosse-Kunstleve, R. W., Jiang, J. S., Kuszewski, J., Nilges, M., Pannu, N. S., Read, R. J., Rice, L. M., Simonson, T., and Warren, G. L. (1998) Crystallography & NMR system: a new software suite for macromolecular structure determination, *Acta Crystallogr., Sect. D: Biol. Crystallogr. 54* (Pt. 5), 905−921.
17. Lamzin, V. S., Wilson, K. S., and Perrakis, A. (2001) Crystallography of biological macromolecules, in *International Tables for Crystallography* (Rossmann, M. G., and Arnold, E., Eds.) pp 720−722, Kluwer Academic Publishers, Dordrecht, The Netherlands.
18. Jones, T. A., Zou, J. Y., Cowan, S. W., and Kjeldgaard (1991) Improved methods for building protein models in electron density maps and the location of errors in these models, *Acta Crystallogr., Sect. A 47* (Pt. 2), 110−119.
19. Laskowski, R. A., MacArthur, M. W., Moss, D. S., and Thornton, J. M. (1993) PROCHECK: a program to check the stereochemical quality of protein structures, *J. Appl. Crystallogr. 26*, 283−291.
20. Betts, L., Xiang, S., Short, S. A., Wolfenden, R., and Carter, C. W., Jr. (1994) Cytidine deaminase. The 2.3 Å crystal structure of an enzyme: transition-state analog complex, *J. Mol. Biol. 235*, 635−656.
21. Ko, T. P., Lin, J. J., Hu, C. Y., Hsu, Y. H., Wang, A. H., and Liaw, S. H. (2003) Crystal structure of yeast cytosine deaminase. Insights into enzyme mechanism and evolution, *J. Biol. Chem. 278*, 19111−19117.
22. Liaw, S. H., Chang, Y. J., Lai, C. T., Chang, H. C., and Chang, G. G. (2004) Crystal structure of *Bacillus subtilis* guanine deaminase: the first domain-swapped structure in the cytidine deaminase superfamily, *J. Biol. Chem. 279*, 35479−35485.
23. Wedekind, J. E., Dance, G. S., Sowden, M. P., and Smith, H. C. (2003) Messenger RNA editing in mammals: new members of the APOBEC family seeking roles in the family business, *Trends Genet. 19*, 207−216.
24. Schaub, M., and Keller, W. (2002) RNA editing by adenosine deaminases generates RNA and protein diversity, *Biochimie 84*, 791−803.
25. Wolfenden, R. (1969) On the rate-determining step in the action of adenosine deaminase, *Biochemistry 8*, 2409−2412.
26. Carlow, D. C., Short, S. A., and Wolfenden, R. (1998) Complementary truncations of a hydrogen bond to ribose involved in transition-state stabilization by cytidine deaminase, *Biochemistry 37*, 1199−1203.
27. Keegan, L. P., Gerber, A. P., Brindle, J., Leemans, R., Gallo, A., Keller, W., and O'Connell, M. A. (2000) The properties of a tRNA-specific adenosine deaminase from Drosophila melanogaster support an evolutionary link between pre-mRNA editing and tRNA modification, *Mol. Cell. Biol. 20*, 825−833.
28. Musier-Forsyth, K., and Schimmel, P. (1992) Functional contacts of a transfer RNA synthetase with 2′-hydroxyl groups in the RNA minor groove, *Nature 357*, 513−515.
29. Ireton, G. C., Black, M. E., and Stoddard, B. L. (2003) The 1.14 Å crystal structure of yeast cytosine deaminase: evolution of nucleotide salvage enzymes and implications for genetic chemotherapy, *Structure (London) 11*, 961−972.
30. Xie, K., Sowden, M. P., Dance, G. S., Torelli, A. T., Smith, H. C., and Wedekind, J. E. (2004) The structure of a yeast RNA-editing deaminase provides insight into the fold and function of activation-induced deaminase and APOBEC-1, *Proc. Natl. Acad. Sci. U.S.A. 101*, 8114−8119.

31. Johansson, E., Mejlhede, N., Neuhard, J., and Larsen, S. (2002) Crystal structure of the tetrameric cytidine deaminase from *Bacillus subtilis* at 2.0 Å resolution, *Biochemistry 41*, 2563−2570.

32. Wilson, D. K., Rudolph, F. B., and Quiocho, F. A. (1991) Atomic structure of adenosine deaminase complexed with a transition-state analog: understanding catalysis and immunodeficiency mutations, *Science 252*, 1278−1284.

33. Terasaka, T., Kinoshita, T., Kuno, M., and Nakanishi, I. (2004) A highly potent non-nucleoside adenosine deaminase inhibitor: efficient drug discovery by intentional lead hybridization, *J. Am. Chem. Soc. 126*, 34−35.

34. Kim, S. H., Quigley, G. J., Suddath, F. L., McPherson, A., Sneden, D., Kim, J. J., Weinzierl, J., and Rich, A. (1973) Three-dimensional structure of yeast phenylalanine transfer RNA: folding of the polynucleotide chain, *Science 179*, 285−288.

35. Shi, H., and Moore, P. B. (2000) The crystal structure of yeast phenylalanine tRNA at 1.93 Å resolution: a classic structure revisited, *RNA 6*, 1091−1105.

36. Saenger, W. (1984) tRNA−a treasury of stereochemical information, in *Principles of Nucleic Acid Structure* (Carter, C. R., Ed.) pp 331−349, Springer-Verlag, New York.

37. Elias, Y., and Huang, R. H. (2005) Biochemical and Structural Studies of A-to-I Editing by tRNA:A34 Deaminases at the Wobble Position of Transfer RNA, *Biochemistry 44*, 12057−12065.

38. Xiang, S., Short, S. A., Wolfenden, R., and Carter, C. W., Jr. (1997) The structure of the cytidine deaminase-product complex provides evidence for efficient proton transfer and ground-state destabilization, *Biochemistry 36*, 4768−4774.

39. Kuratani, M., Ishii, R., Bessho, Y., Fukunaga, R., Sengoku, T., Shirouzu, M., Sekine, S., and Yokoyama, S. (2005) Crystal structure of tRNA adenosine deaminase (TadA) from *Aquifex aeolicus*, *J. Biol. Chem. 280*, 16002−16008.

40. Losey, H. C., Ruthenburgh, A. J., and Verdine, G. L. (2006) Crystal structure of *Staphylococcus aureus* tRNA adenosine deaminase TadA in complex with RNA, *Nat. Struc. Mol. Biol. 13*, 153−159.